Capabilities of the GAMMA-400 gamma-ray telescope to detect electron + positron flux at TeV-energies from lateral directions

V.V. Mikhailov[a,*], A.M. Galper[a,b], N.P. Topchiev[b], I.V. Arkhangelskaja[a], A.I. Arkhangelskiy[a], A.V. Bakaldin[c], I.V. Chernysheva[a], O.D. Dalkarov[a], A.E. Egorov[b], M.D. Kheymits[a], M.G. Korotkov[a], A.A. Leonov[a,b], A.G. Malinin[a], A.G. Mayorov[a], A.V. Mikhailova[a], P.Yu. Minaev[b,d], N.Yu. Pappe[b], S.I. Suchkov[b], Yu.T. Yurkin[a]

[a]*National Research Nuclear University "MEPhI" (Moscow Engineering Physics Institute),*
  Kashirskoe shosse, 31, Moscow, Russian Federation

[b]*Lebedev Physical Institute of the Russian Academy of Sciences,*
  Leninskiy Prospekt, 53, Moscow, Russian Federation

[c]*Scientific Research Institute for System Analysis of the Russian Academy of Sciences,*
  Nakhimovsky prospekt, 36/1, Moscow, Russian Federation

[d]*Space Research Institute,*
  Profsoyuznaya Str., 84/32, Moscow, Russian Federation

  E-mail: vvmikhajlov@mephi.ru, aaleonov@mephi.ru

The future space-based GAMMA-400 scientific observatory is being developed under the Federal Space Program of Russian Federation in the period from 2016-2025. This observatory includes a γ-ray telescope, which will detect gamma rays in the energy range from ~20 MeV to several TeV with high angular and energy resolutions and cosmic-ray electrons + positrons up to several tens of TeV using main and lateral appertures. Recent experimental observations indicate a possible existence of a break in the electrons + positrons spectrum at around TeV energies. A number of speculations to explain this phenomenon have arisen. This article presents the method of high-energy electrons detection from the lateral aperture of the GAMMA-400 gamma-ray telescope. This method implements the machine learning analysis and provides the high-energy proton background rejection at the level of 10^4 in the energy range from 100 GeV to 10 TeV. The effective acceptance for electron detection with such proton rejection is about 0.52 $m^2 \times sr$ for the four lateral sides of the GAMMA-400 gamma-ray telescope. This effective acceptance exceeds by several times that of CALET and DAMPE experiments. This capability of our instrument will allow us to improve significantly the measurements of electron + positron flux above 1 TeV and, hence, understand better the debatable spectrum break.

---

*Speaker

1.   Introduction

Recent measurements of total spectrum of cosmic-ray electrons and positrons in TeV energy range were reported by the space experiments DAMPE [1], CALET [2,3], FERMI-LAT [4], AMS-2 [5], PAMELA [6]; the ground-based telescopes H.E.S.S. [7], MAGIC [8], VERITAS [9] and by the balloon-based instrument ATIC [10]. The spectrum exhibits a softening of the power-law index at about 1 TeV, as it was observed for the first time by H.E.S.S., and confirmed by DAMPE and CALET with a high significance of 6.6σ [1, 3, 7]. This spectrum feature could be produced by a single, local and fading source, accelerating electrons up to several TeV energies. Other plausible explanations include the stochastic distribution of sources or the electron leakage from the Galactic disk [11-14]. The positron spectrum with a likely reduction in flux above ~400-500 GeV can be explained only if the local sources of TeV particles do not produce electrons and positrons in equal amount [14]. Moreover, the effect of possible energy scale uncertainties of the experiments has to be taken into account [15].

Besides an improvement in statistics, it is necessary to expand the energy range of detection up to ~10–20 TeV in order to clarify the electron spectrum behavior at energies more than 1 TeV. Another advantage of such an expansion into the TeV energy range is to explore the possibility of observing the anisotropy in electron flux, because the influence of galactic magnetic fields is practically insignificant at such energies. In case of anisotropy detection, the position of a local source could be found, if this source exists.

The gamma-ray telescope GAMMA-400 [16-18], which is being developed currently, designed to measure gamma rays in the energy range from ~20 MeV to several TeV and cosmic-ray (CR) electrons + positrons up to several tens of TeV. The telescope will survey the Galactic plane and Galactic center in details with high-energy (~2% at 100 GeV) and angular (~0.01^0 at 100 GeV) resolutions. Our telescope has a significant lateral aperture [19], which provides the possibility to detect electrons + positrons with good energy resolution up to ~10−20 TeV thanks the thickness of GAMMA-400 calorimeter in transverse direction (~43 X_0).

As known, the bulk of cosmic rays are protons and helium nuclei, whereas the lepton fraction in the total flux is ~10^{-3} at high energies [14]. In the present paper, the simulated capability of the GAMMA-400 telescope to distinguish electrons and positrons from protons in CRs in lateral aperture is addressed. The values of proton rejection coefficient and the acceptance for electrons + positrons detection in the energy range from 100 GeV to 10 TeV are presented.

2 The physical scheme of the GAMMA-400 gamma-ray telescope

The GAMMA-400 instrument consists of the anticoincidence system (AC top, AC lat), the converter-tracker (C), the time-of-flight (ToF) system from the detectors S1 and S2, the position-sensitive calorimeter (CC1), the electromagnetic calorimeter (CC2), the detectors S3 and S4 located above and behind the CC2 calorimeter, and lateral detectors (LD) surrounding the CC2 calorimeter. Figure 1 schematically shows the structure of the GAMMA-400 gamma-ray telescope. The arrow indicates one of the lateral sides, from which the detection of electrons + positrons is considered herein. The information from CC2, LD, S3 and S4 detectors is used for particle identification.

The CC2 electromagnetic calorimeter consists of 22×22 CsI(Tl) crystals. Each crystal has dimensions of $36 \times 36 \times 300$ mm^3. The thickness of CC2 is 16 X_0 (~0.9 λ_0) for vertical incidence and 43 X_0 (~2 λ_0) for lateral detection. Each of four lateral detectors LD has two layers

POS(ECRS)155

formed by scintillation plates oriented along CsI(Tl) crystals. Their size is $117 \times 10 \times 380$ mm^3. The scintillation detectors S3 and S4 have the similar two-layer structure and are made of scintillation plates having with the size $1000 \times 100 \times 10$ mm^3. The detailed description of the GAMMA-400 detectors can be found in [18].
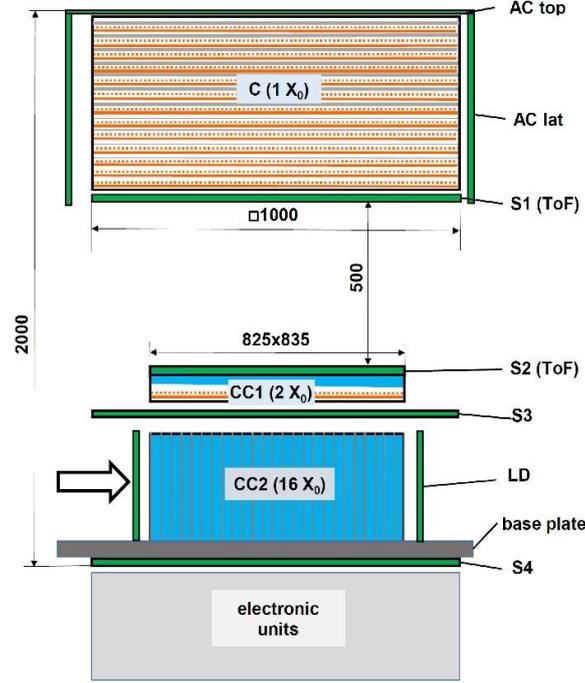

Figure 1: Schematic drawing of the GAMMA-400 telescope.

Simulations of the GAMMA-400 performance were carried out using the program software GEANT 4.10 [20]. An example of simulation of 3-TeV electron energy release in the gamma-ray telescope detectors is shown in Figure 2, where detectors are shown by color, if the response exists. The incidence direction of electron is shown by the arrow. Two projections of the gamma-ray telescope response are shown at the top of the Figure 2. At the bottom, a view from above CC2 together with the anticoincidence system (AC lat) detectors and legend for the values of energy release are shown.

3 The methods of proton rejection while detecting electrons + positrons in the energy range from 100 GeV to 10 TeV from lateral directions.

The main task while detecting high energy electrons + positrons is to put away the influence of background from predominantly protons. In principle, an interacting proton with energy more than E_0 could imitate an electron with energy E_0, since the proton may release the same energy deposit in the GAMMA-400 calorimeter. To estimate the probability of such proton rejection, the isotropic fluxes of electrons with energy E_0 and of protons with energies more than E_0, assuming that the proton energy spectrum power-index is 2.7, were simulated on the surface of LD detector as shown by the arrow in Figure 1. The rejection factor of protons for the electron energy E_0 is then calculated as the ratio of electron efficiency to the proton efficiency.

The main trigger for particle detection is the following:

$$(E_{CC2} > E_{CC2}^{Threshold}) \,\&\, (E_{LD} > E_{LD}^{Threshold}) \tag{1},$$

where E_{CC2} is the signal, induced by initial particle energy release in CC2;

E_{LD} is the signal, induced by initial particle energy release in one among four detectors LD;

$E_{CC2}^{Threshold}$ is the threshold for the value of signal in CC2;

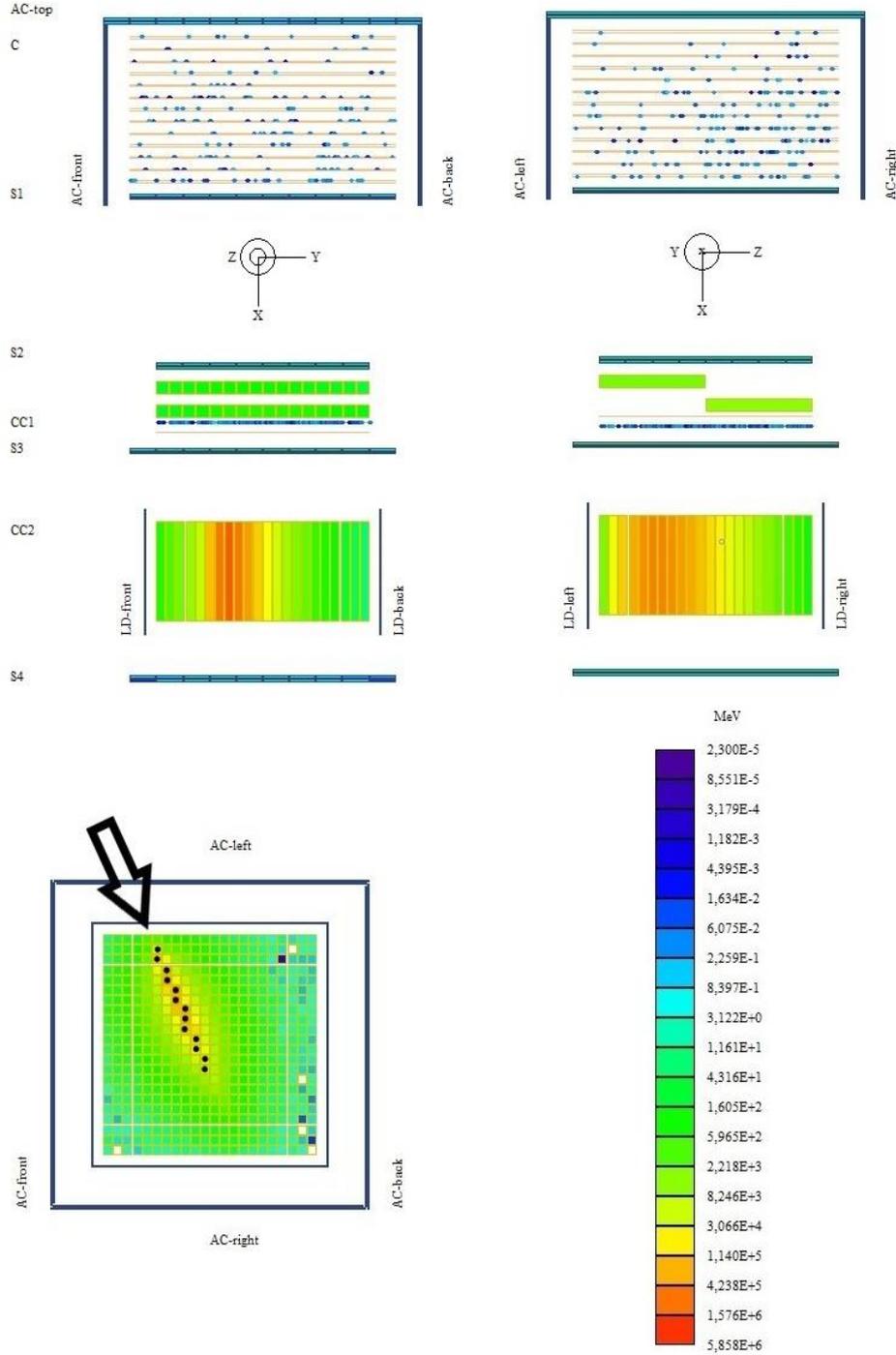$E_{LD}^{Threshold}$ is the threshold for the value of signal in LD.

Figure 2: An example of simulation of 3-TeV isotropic electron energy release in the gamma-ray telescope detectors. Top: two projections of the gamma-ray telescope response. Bottom: a view from above CC2 together with anticoincidence system (AC lat) detectors and legend for the values of energy release.

Since the main point concerns the detection of high-energy electrons, the value of $E_{CC2}^{Threshold}$ was chosen to be equal to 80 GeV in order to avoid a high load of GAMMA-400 telescope trigger

system from protons with energies less than 100 GeV. The value $E_{LD}^{Threshold}$ was set equal to 0.3 MIP (minimum ionizing particle) or equvalently 0.6 MeV to reliably distinguish charged particles from gammas reliably [21].

On the first step of the event analysis the track reconstruction was performed. The construction of calorimeter CC2 from CsI(Tl) crystals provides the possibility to restore energy deposit lengthwise the track in 2D plane only (Fig. 2). The track is built along the rows of CsI(Tl) crystals. These rows are formed virtually along LD detector, which is hit by an initial particle. In each $i - th$ row $j - th$ the crystal with the maximum $E_{i,j}^{max}$ the crystal with the maximum signal is determined. The track is considered to be passing through the selected crystal, if the following conditions are fulfilled jointly:

$$E_{i,j}^{max} + E_{i,j-1} + E_{i,j+1} > 0.8 \times \sum_j E_{i,j} \qquad (2),$$
$$E_{i,j}^{max} > 0.01 \times \sum_{i,j} E_{i,j} \qquad (3),$$

where j is the number of CsI(Tl) crystal in $i - th$ row

The coefficients in the relations (2, 3) were obtained from the requirement of maximum efficiency for electron track reconstruction. The condition (2) extracts the parts of the track in CC2, where the electromagnetic cascade along the shower axis is already developed. The condition (3) provides, in addition, the possibility to reject the parts of the track with low value $E_{i,j}^{max}$. In Figure 2 the points of restored track are marked by the black dots.

The accuracy of initial energy reconstruction has to be provided during the analysis of the topology of shower induced by charged particles. For this purpose the events taken off from CC2 through lateral crystals are checked additionally to the following condition:

$$(E_{CC2} > E_{CC2}^{Threshold}) \,\& \,(E_{LD} > E_{LD}^{Threshold}) \& (N_{Track} > 8) \& (N_{Track}^{Lateral} = 0) \qquad (4),$$

where N_{Track} is the number of CsI(Tl) crystals being in restored track according to criterions (2) and (3); $N_{Track}^{Lateral}$ is the number of lateral CsI(Tl) crystals of CC2 being in restored track.

The threshold value for N_{Track} is deduced from the fact that electrons with initial energy 80 GeV, which hit the central part of calorimeter crystal from the normal direction, have the track consisting of at least eight CsI(Tl) crystals. In Figure 2 the lateral CsI(Tl) crystals of CC2 are front, right and back.

When calculating the rejection factor of protons, apart from the standard methods for track reconstruction and analyzing, the machine learning approach was applied. Namely, the algorithm of gradient boosting machine [22], which is used in addition to BDT (Boosted Decision Tree) method to improve the accuracy of classification, was applied. This algorithm is realized in ROOT 6.22/08 [23] software. The input data for the machine learning algorithm were formed from the results of GEANT 4 simualtion. They include the signals in gamma-ray telescope detector systems and combinations of these signals, which arise as a response due to primary electron or proton incidence from lateral directions. For each electron or proton event, a set of thirty parameters was created. The most important parameters are:

the number of CsI(Tl) crystals in CC2 with a signal more than $E_{CC2}^{Threshold} = 80 \; GeV$;

the value of maximum signal among the crystals present in the reconstructed track;

the ratio of maximum signal among the crystals present in the reconstructed track to the number of track points (crystals) from the track beginning to the point with maximum signal;

the maximum of RMS for signals among the layers of CsI(Tl) crystals in CC2;

5

the number of layer of CsI(Tl) crystals, which contains the crystal with maximum signal;
the value of sum of the signals in the first layer of CsI(Tl) crystals;
the value of sum of the signals in the last layer of CsI(Tl) crystals.

In Figure 3 the distributions for proton and electron events, satisfying condition (4), when calculating the proton rejection factor for 3-TeV electrons are shown. The distributions over the value of maximum signal in the CsI(Tl) crystals are presented in Figure 3a. The distributions over the value of classification parameter are shown in Figure 3b. From Figure 3b it is seen, that the employed machine learning algorithm provides a good separation between proton and electron events.
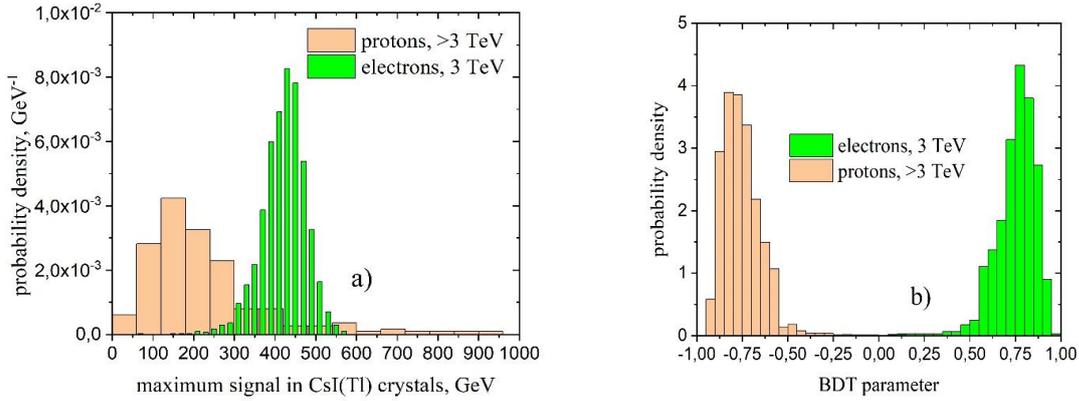

Figure 3: The distributions for proton and electron events, which satisfy condition (4), for the case of calculating the proton rejection factor for 3 TeV electrons. The distribution for the value of maximim signal in the CsI(Tl) crystals (a). The distributions over the value of classification parameter (b).

The distribution over energy release in CC2 for 3 TeV electrons, which survived after BDT analysis, is shown in Figure 4a by the black columns. To improve further the accuracy of energy reconstruction for selected electron events, the signals from S3 and S4 detectors are used.
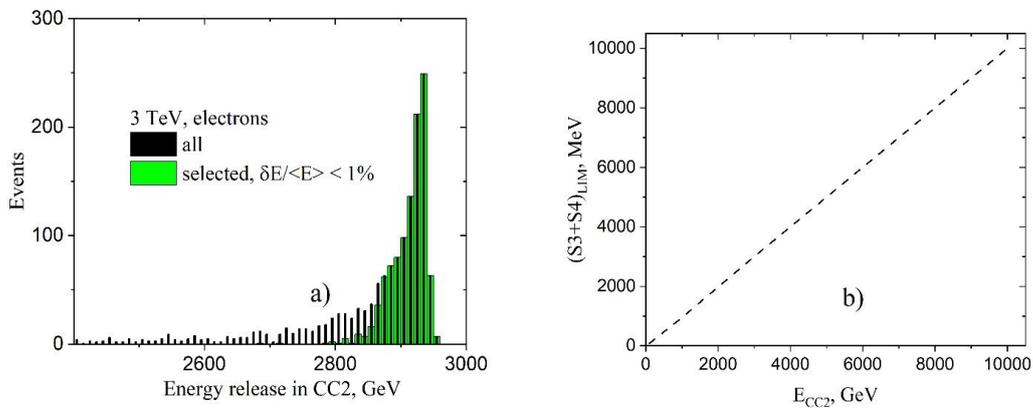

Figure 4: The distributions over energy release in CC2 for 3 TeV electrons, survived after BDT analysis only (black columns), and satisfying the additional "S3+S4 selection" (green columns) (a). The dependence of threshold value for total energy release in S3 and S4 detectors from the energy release in CC2 (b).

To improve energy reconstruction, one can use the value of threshold for total energy release in S3 and S4 detectors to extract the part of events, for which a leakadge is small, and the energy is well reconstructed. The data of simulation allows us to obtain the dependence of threshold value for total energy release in S3 and S4 detectors on the energy release in CC2 (Fig. 4b). If the value of total energy release in S3 and S4 detectors is less than threshold value for some electron event with the given energy release in CC2, then the energy of this event is well reconstructed, and the event is retained for the scientific use. The distribution over energy release in CC2 for 3 TeV electrons, survived after BDT analysis and descrided as "S3+S4 selection", is shown in Figure 4a by the green columns. The energy resolution for the remainig events is about 1%. The procedure of this additional selection was applied for all events, and was taken into account in proton rejection factor and electron acceptance calculations.

4 Results

The values of the proton rejection factor and the electron acceptance of one lateral side for eneries in the range from 100 GeV to 10 TeV, while detecting by lateral aperture of GAMMA-400 gamma-ray telescope, are presented in Table 1. It is seen, that when using the lateral apperture of GAMMA-400, it is possible to provide proton rejection from electorns at the level of 10^4. The total value of electron acceptance (for all lateral sides) reaches ≈ 0.52 m$^2\times$sr. This value exeeds the electron acceptance of DAMPE [1] and CALET [2] experiments at TeV energies by about five times. Using the data of CALET [2] and obtained acceptance of GAMMA-400, it is possible to estimate that the number of detected electorns + positrons in the energy range from 1 to 4.5 TeV during GAMMA-400 operation will be $4\times160=640$ e$^-$ per year.

Energy, TeV	0.1	0.5	1	3	5	10
Proton rejection factor $\times10^{-3}$	16±5	17±5	17±6	15±4	12±3	12 ±3
Electron acceptance, cm$^2\times$sr	1175±15	1310±20	1370±30	1380±30	1370±40	1380±50

Table 1. The values of proton rejection factor and electron acceptance.

Acknowledgements

References

[1] G. Ambrosi, et al., *Direct detection of a break in the teraelectronvolt cosmic-ray spectrum of electrons and positrons, Nature* (2017), 552, 63-66.

[2] O. Adriani, et al., *Extended measurement of the cosmic-ray electron and positron spectrum from 11 GeV to 4.8 TeV with the calorimetric electron telescope on the international space station, PRL* (2018), 120, 261102, 1-7.

[3] P.S. Marrocchesi, et al., *New Results from the first 5 years of CALET observations on the International Space Station, Proceedings of 37th International Cosmic Ray Conference.PoS(ICRC2021)010* https://pos.sissa.it/395/010/pdf.

[4] S. Abdollahi, et al., *Cosmic-ray electron-positron spectrum from 7 GeV to 2 TeV with the Fermi Large Area Telescope, Phys. Rev. D* (2017), 95, 082007.

[5] M. Aguilar, et al., *Precision measurement of the (e^+ + e^-) flux in primary cosmic rays from 0.5 GeV to 1 TeV with the Alpha Magnetic Spectrometer on the international space station, PRL* (2018), 120, 261102, 1-7.

[6] V. V. Mikhailov, et al., *Galactic Cosmic Ray Electrons and Positrons over a Decade of Observations in the PAMELA Experiment, Bulletin of the Russian Academy of Sciences: Physics*, (2019) 83, 8, 974–976V.

[7] F. Aharonian, et al.*, Energy spectrum of cosmic-ray electrons at TeV energies, PRL* (2008), 101, 261104, 1-5.

[8] D. Borla Tridon, et al., *Measurement of the cosmic electron plus positron spectrum with the MAGIC telescopes, Proceedings of 32nd International Cosmic Ray Conference,* (2011), 47-50.

[9] A. Archer, et al., *Measurement of cosmic-ray electrons at TeV energies by VERITAS, Phys. Rev.* (2018), D 98, 062004, 1-7.

[10] J. Chang, et al., The ATIC Collaboration, An excess of cosmic ray electrons at energies of 300–800 GeV, Nature (2008) 456, 362.

[11] S. Recchia, et al., *Local fading accelerator and the origin of TeV cosmic ray electrons, Phys. Rev.* (2019), D 99, 103022, 1-6.

[12] P. Lipari, *Spectral shapes of the fluxes of electrons and positrons and the average residence time of cosmic rays in the Galaxy, Phys. Rev.* (2019), D 99, 043005, 1-28.

[13] P. Mertsch, *Stochastic cosmic ray sources and the TeV break in the all-electron spectrum, J. Cosmol. Astropart. Phys.* (2018), 11, 045.

[14] S. Gabici et al, *The origin of Galactic cosmic rays: Challenges to the standard paradigm, International Journal of Modern Physics D,* (2019),28, 15, 1930022 DOI: 10.1142/S0218271819300222

[15] Yu-Chen Ding et al. *Implications of a possible TeV break in the cosmic-ray electron and positron flux, Phys. Review D* (2021) 103, 115010

[16] A. Galper, et al., *Status of the GAMMA-400 project, Adv. Space Res.* (2013), 51, 297-300.

[17] A. Galper, et al., *GAMMA-400 project, Astron. Rep.* (2018), 62, 882-889.

[18] N. Topchiev, et al., *Gamma- and Cosmic-Ray observations with the GAMMA-400 gamma-ray telescope, Adv. Space Res.* (2022), 70, 2773-2793.

[19] A. Leonov, et al., *Capabilities of the GAMMA-400 gamma-ray telescope to detect gamma-ray bursts from lateral directions, Adv. Space Res.* (2022), 69, 514-530.

[20] *https://geant4.web.cern.ch/support/user_documentation.*

[21] A. Arkhangelskiy, et al., *Event selection system of the GAMMA-400 gamma-ray telescope, Bulletin of the Russian Academy of Science: Physics* (2021), 85, 8, 1160-1164.

[22] J.H. Friedman, *Greedy function approximation: a gradient boosting machine, Ann. Statist.,* (2001), 29, 5, 1189-1232.

[23] *https://root.cern.ch/root/htmldoc/guides/users-guide/ROOTUsersGuide.html.*

PoS(ECRS)155